Laboratory experiments on the effect of baroclinic eddies on a dense plume in a rotating stratified fluid

Danielle Wain

1 Introduction

Eighteen degree water (EDW) is a subtropical mode water of the North Atlantic. Mode water is a layer of water with vertically constant temperature and salinity. It often forms near strong baroclinic fronts, which provide a mechanical forcing for its creation and properties, in regions of high air-sea interaction, a buoyant forcing. Figure 1 shows the region of high wintertime net heat flux, which corresponds with the location of the EDW. This region of large heat flux is located near the Gulf Stream, a strong baroclinic front. Figure 2 shows the mode water. The left panel shows the temperature and velocity in this region. The thick layer of constant temperature can be seen here as well as the front from the Gulf Stream. The center panel shows the constant salinity layer and the isopycnals, which clearly show the mode water. The right panel shows the historical formation of the EDW predicted from air-sea fluxes, which in recent times has ranged between 15 and 25 Sv [1]. But Kwon and Riser inferred that 4 Sv is injected into the subtropical gyre[2]. The discrepancy between the estimated and the observed values is currently under investigation. The goal of these experiments is to investigate if lateral eddy fluxes by the eddies created by the baroclinic front of the Gulf Stream could explain the discrepancy. In the current experiments, a baroclinic front was created via upwelling and a dense line plume was injected at the surface to simulate the processes under which the EDW is formed. From hereafter, a line plume is defined as a plume that is driven by a buoyancy flux per unit length on a line whose extent in one horizontal direction is much larger than in the other horizontal direction, whereas a point plume is emitted from a single point.

The EDW formation process was simulated as a line plume in a rotating linearly stratified fluid. In a non-rotating flow, Rouse et al. examined the case of a line plume in a homogeneous fluid[4]. Morton et al. developed a theory for convection for both continuous and instantaneous point sources for an arbitrary stratification (including the homogeneous case), with a detailed analysis for the linearly stratified case[5]. Wright and Wallace experimentally examined the behavior of a line plume in a linearly stratified fluid[6]. Other previous experimental work on plumes in stratified fluids includes that of Noh et al. and Ching et al., who examined respectively a thermal and a negatively buoyany turbulent line plume descending through a two-layer fluid with a sharp density interface[7][8]. Laboratory experiments on the effect of rotation on a bouyant line plume in a homogeneous fluid were conducted by Fernando and Ching[9]. Lavelle and Smith studied this effect numerically

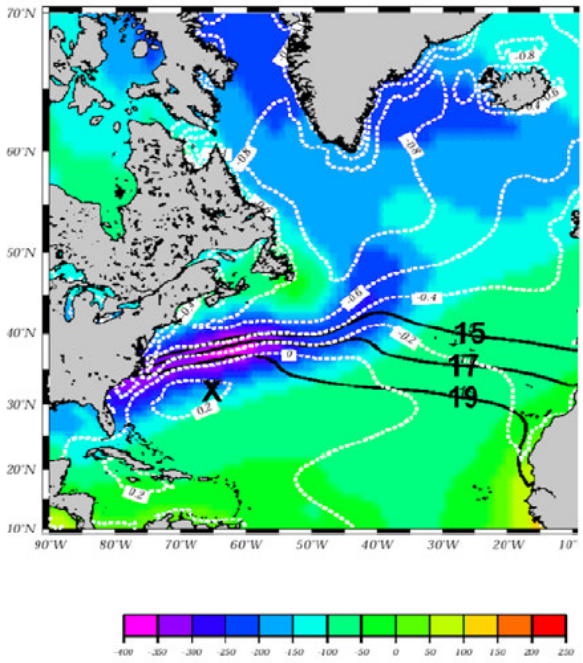

Figure 1: Wintertime net heat flux over the North Atlantic (Steve Riser, from John Marshall, pers. comm.).

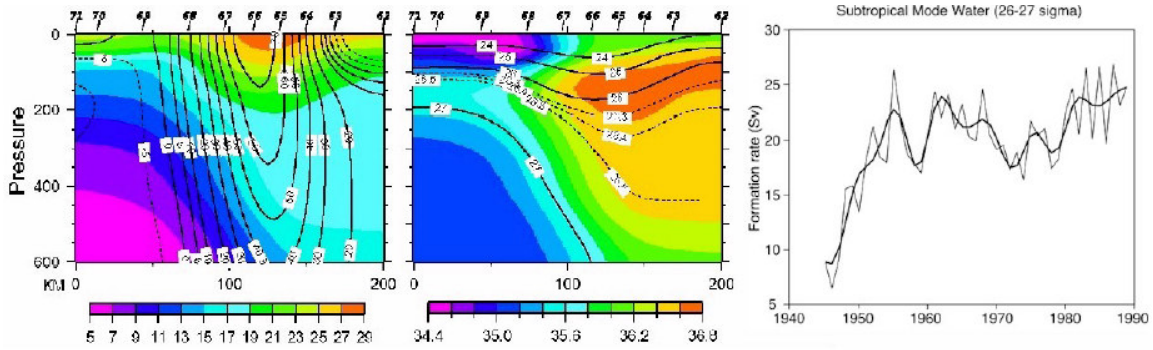

Figure 2: Meridional sections across the Gulf Stream of temperature and velocity(left) and salinity and potential density (center) (from Joyce[3]). The right panel shows the formation rate of the subtropical mode water estimated from air-sea fluxes.

using a three-dimensional nonhydrostatic model[10]. Fernando et al. performed laboratory experiments on the development of a dense turbulent point plume in a rotating homogeneous fluid[11]. More recently, Bush and Woods experimentally investigated the vortices produced by a buoyant line plume in both a homogeneous and a linearly stratified flow[12]. The rotating stratified case for a point plume has been studied by Helfrich and Battisti, who conducted laboratory experiments studying the effect of rotation on a hydrothermal plume[13], and Speer and Marshall, who conducted numerical experiments on the convection produced by a buoyant point source in a linearly stratified fluid[14].

The previous work on plumes most relevant to the current study is the experiments of Bush and Woods on a line plume in a rotating linearly stratified fluid. From their experiments, they found that the height of intrusion of the plume was

$$Z_n = (3.0 \pm 1.0)\frac{(B/L)^{1/3}}{N}, \tag{1}$$

where B is the total buoyancy flux, L is the length of the source, and N is the buoyancy frequency (which is constant in a linearly stratified fluid)[12]. The coefficient is similar to the value of 2.5 found by Wright and Wallace[6]. The reduced gravity of the intrusion in their experiments was

$$g_i' = g\frac{\rho_i - \rho_b}{\rho_b} \tag{2}$$

where ρ_i is the density of the intrusion and ρ_b is the density at the bottom of their tank (where the injection occurred in their experiments). They did not measure the density of the intrusion but predicted that it scaled as

$$g'(Z_n) \sim (B/L)^{1/3}N. \tag{3}$$

Manipulation of their scaling for the size of the eddies formed by the plume gives an eddy radius that scales as

$$R_{plume} \sim NZ_n/f,$$

where f is the Coriolis parameter.

Others have performed experiments investigating the eddies formed from fronts created by upwelling. In these experiments the eddies are created by instabilities at the front. For example, Narimousa and Maxworthy studied a two layer fluid where upwelling was forced by a disk spinning on the surface of the fluid[15]. In these experiments they found the velocity on the surface was

$$V = 0.74r\Delta\Omega, \tag{4}$$

where r is the radius of the disk and $\Delta\Omega$ is the rotation rate of the disk (with respect to the fluid). In other experiments, eddies were observed that scaled with the Rossby radius of deformation:

$$R = NH/f, \tag{5}$$

where H is the depth of the fluid[16].

The current experiments examined the effect of these eddies created by upwelling on the dense plume injected into a linearly stratified rotating fluid.

2 Experiment

The experiments were conducted in circular tank with a diameter of 115 cm positioned in the center of a 2 m rotating table. A disk with a radius r of 13 cm was suspended over the center of the tank at a height of 31 cm above the bottom. The linear salt stratification was created using the double-bucket method. The tank was filled while rotating until the disk was resting on the surface of the water. During filling and spin-up, the tank was covered with cellophane to minimize wind stresses. The tank rotated counterclockwise and the disk rotated in the same direction. The dense salty water for the plume was dyed green for visualization and injected via a perforated copper pipe ring that encircled the disk. The pipe was covered in foam to evenly distribute the dense fluid. In contrast to the experiments of Bush and Woods, a dense plume was injected at the surface rather than a buoyant plume injected on the bottom. For each experiment, the dense water was injected in 10 - 12 bursts of 20 - 30 seconds each. As discussed in Bush and Woods, there are several "instability times" that define the number of eddies created from the plume. The injection time was limited to the first instability time so that the eddies could be more easily observed. The multiple injections also simulated the more realistic sporadic atmospheric forcing that would create EDW. A conductivity probe measured the water column to get density profiles during the experiments. A camera was mounted on the rotating table that photographed the development of the plume from a sideview. A camera mounted above the table that rotated at the same rate videotaped the plume from above. A syringe pump was used to inject blue dye lines on isopycnals so that upwelling could be observed. Figures 3 and 4 show plan and side views of the experimental setup respectively. Figures 5,6, and 7 show photographs of the experimental setup. The variable parameters in the experiments were the flow rate of the dense water Q $(10 - 37.5\ cc\ s^{-1})$, the reduced gravity of the dense water g'_s $(1.1 - 100\ cm\ s^{-2})$, the disk rotation $\Delta\Omega$ $(0.149 - 3.190\ rad\ s^{-1})$, the buoyancy frequency N $(0.205 - 1.022\ rad\ s^{-1})$, and Coriolis parameter f $(0.8 - 2\ rad\ s^{-1})$.

Figure 4 also shows how the height of the eddies was determined. Geostrophy states that the azimuthal velocity V is

$$V = \frac{g'}{f}\frac{dh}{dx}, \tag{6}$$

where dh/dx is the slope of the isopycnals and is equivalent to S as depicted in Figure 4. Rearranging and scaling g' as N^2H, V as $r\Delta\Omega$ as in Narimousa and Maxworthy, and using Equation 5, h_e can be scaled as

$$h_e = SR = \frac{r\Delta\Omega}{2N}. \tag{7}$$

Note the factor of 1/2. The velocity on the bottom was zero. In this scaling, the average velocity, rather than the surface velocity, was the velocity of interest, so this factor was

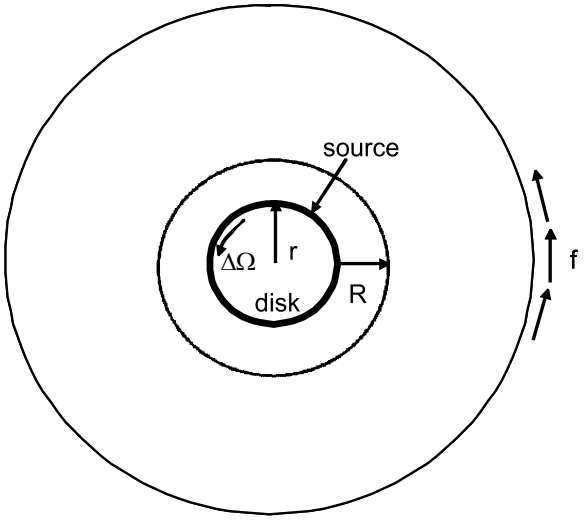

Figure 3: Plan view of the experimental setup.

added. Measurements of the slope from photographs (see Figure 8) show that the above scaling for the slope is accurate within 30%.

3 Theory

The behavior of the dense plume is function of a combination of the vertical buoyancy flux from the plume and the lateral eddy buoyancy flux due the eddies created by the upwelling front. An appropriate scaling needs to be determined for both fluxes. The ratio of these terms should provide insight into the plume behavior. The buoyancy flux is commonly defined as

$$B = g'_s Q, \tag{8}$$

where Q is the volumetric flow rate of the source and g'_s is defined here as

$$g'_s = g\frac{\rho_{source} - \rho_{top}}{\rho_{top}} \tag{9}$$

where ρ_{source} is the density of the source water for the plume and ρ_{top} is the density at the surface of the tank, where the plume is injected.

The lateral eddy buoyancy flux can be written as

$$M = \overline{v'b'} \times 2\pi\frac{2r + R}{2}h_e \tag{10}$$

where $\overline{v'b'}$ is the lateral buoyancy eddy flux per unit area. In this equation, the area through which the flux acts is defined as the height of the eddies created via upwelling (see Figure 4) times the perimeter of the circle through which the flux acts. Here this perimeter is defined as the average between the circle created by the disk and the circle created by the eddies (of radius R - see Figure 3) generated at the edge of the disk. Using a flux-gradient relationship,

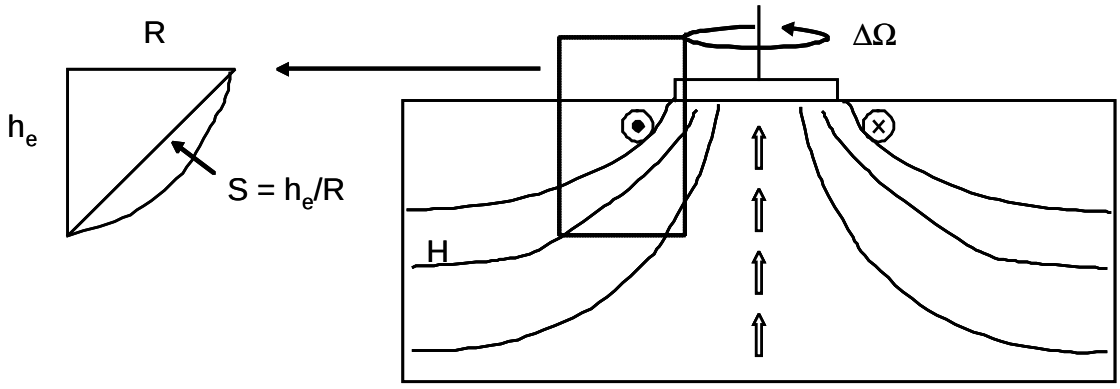

Figure 4: Side view of the experimental setup. The section shown indicates how the height of the eddies was scaled.

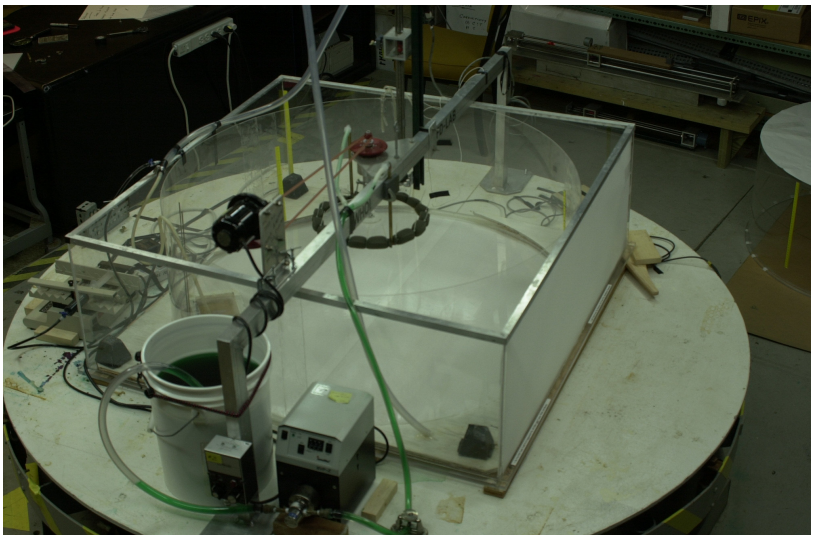

Figure 5: Overhead view of experimental setup. In the foreground the pump that delivers the source can be seen.

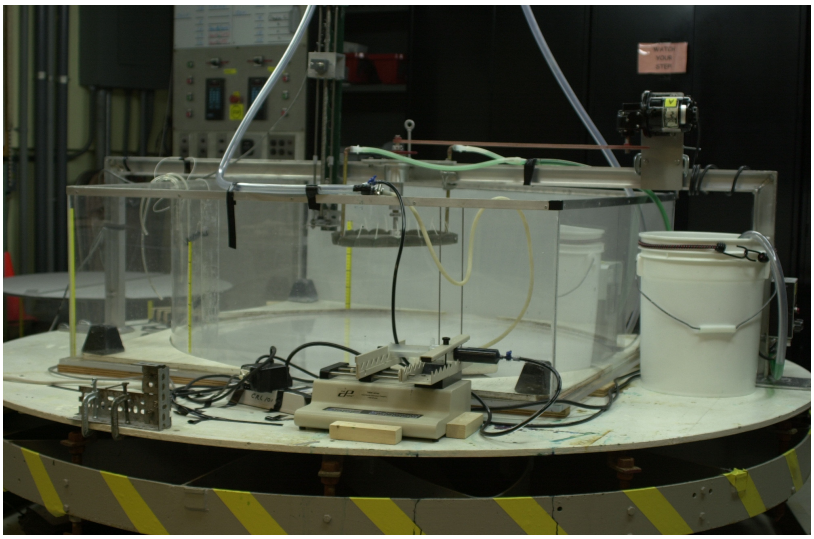

Figure 6: Side view of experimental setup. In the foreground the syringe pump that was used to inject dye lines for visualization of the upwelling can be seen.

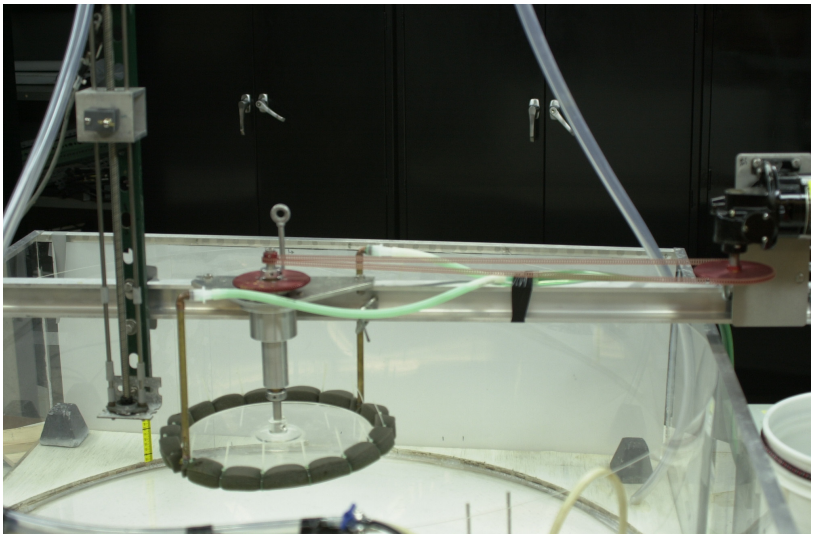

Figure 7: View of the disk that is rotated to create upwelling and the piping that delivers the source. The profiling apparatus for the conductivity sensor is seen to the left of the disk.

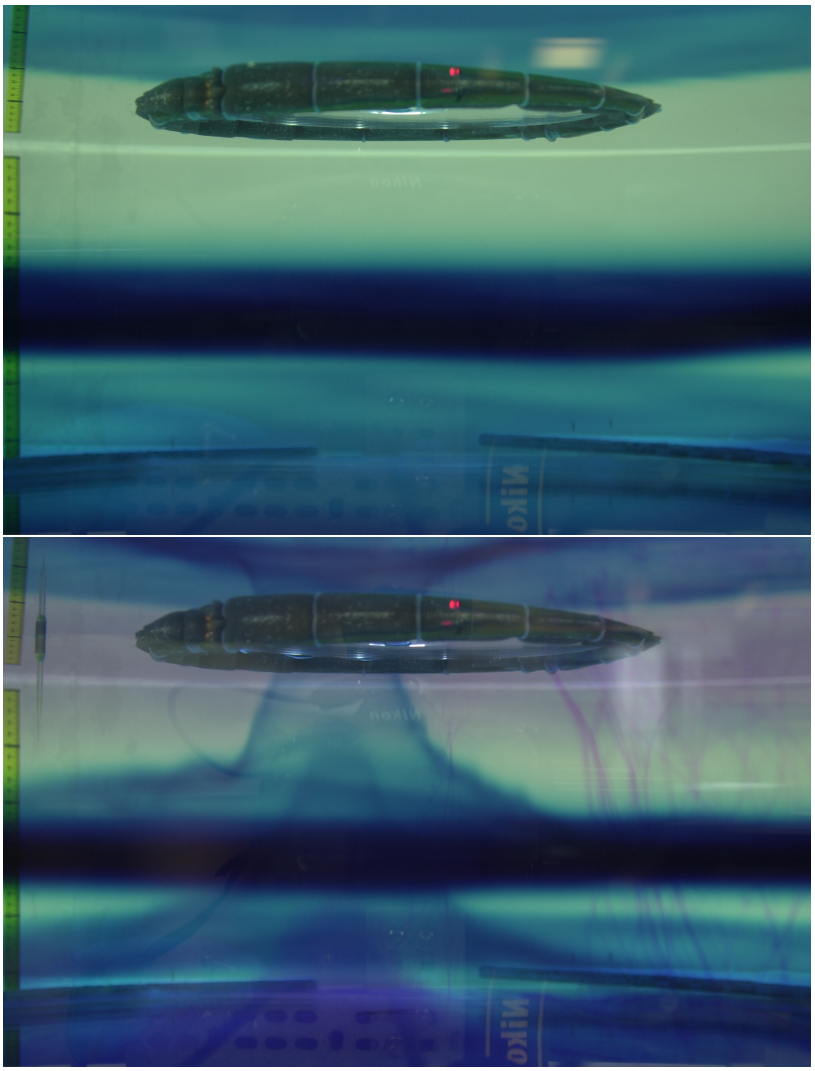

Figure 8: Upwelling in the current experiment. The upper photo shows the isopycnals before the disk starts rotating and the lower panel shows the sloping of the isopycnals.

$$\overline{v'b'} = -K\nabla b, \tag{11}$$

where K is an eddy diffusivity. The eddy diffusivity can be described as

$$K = cVR, \tag{12}$$

where c is an eddy efficiency parameter. Cenedese et al. and others found that the value of the eddy efficiency parameter ranged between 0.01 and 0.06[17]. In the current experiments a value of $c = 0.05$ was used. ∇b can be scaled as $-\Delta b/R$, where b is assumed to change over the lengthscale R. Assuming Δb scales as N^2H (or g') and using Equation 12, the lateral buoyancy flux per unit area is

$$\overline{v'b'} = cVN^2H \tag{13}$$

Using Equations 5 7, and 13 and the scaling for V from Narimousa and Maxworthy (including a factor of 1/2 as stated above), Equation 10 can be rewritten as

$$M = \frac{c\pi}{4}\left(r\Delta\Omega\right)^2 NH\left(2r + \frac{NH}{f}\right). \tag{14}$$

In the current experiments the effect of the ratio B/M on the plume behavior was examined:

$$\frac{B}{M} = \frac{g'Q}{\frac{c\pi}{4}\left(r\Delta\Omega\right)^2 NH\left(2r + \frac{NH}{f}\right)}. \tag{15}$$

It was hypothesized that when $B/M < 1$, there would be a significant lateral buoyancy flux would overwhelm the vertical buoyancy flux; when $B/M = 1$, the source and lateral eddy flux have similar strength so they are both relevant for plume dynamics; and when $B/M > 1$, the plume would behave as in the experiments of Bush and Woods due to the negligible value of the lateral eddy flux. It was also hypothesized that an effective vertical buoyancy flux, which would account for lateral eddy flux could be defined as

$$B* = B - M, \tag{16}$$

which can be rearranged to give

$$B* = B\left(1 - \frac{M}{B}\right). \tag{17}$$

4 Results

First, the plume behavior was qualitatively analyzed. Overhead video of the experiments showed a distinct difference in the size of the eddies between the experiments with and without upwelling (with all other parameters held constant). First, the base case with no upwelling is examined. Figure 9 shows the plume (in green) after the first injection of dense fluid (upper photo) and after five injections (lower photo). The eddies formed

from the injection can clearly be seen in the upper photo. After several injections a thin layer formed. Figure 10 compares the base case with no upwelling (upper photo) with the upwelling case (lower photo). The eddies created by the upwelling affect the plume by causing it to mix as it sinks, resulting in a thicker mixed layer whose midpoint is not as deep as that formed with no upwelling. The eddies essentially increase the entrainment of the ambient fluid into the plume as it descends.

The measured density profiles provided a mechanism for a quantitative analysis of the intrusion of the plume. In the current experiments, the depth of the midpoint of the intrusion, the average density of the intrusion, and the thickness of the intrusion were investigated as a function of B/M. Figure 11 shows a typical density profile after the injection of the plume (without upwelling). The plume creates a step in the background density profile, which would be expected based on comparison with the upper photo of Figure 10. Figure 11 also shows the depth that Equation 1 predicts the plume will descend to. Note that this distance was assumed to start at the bottom of the mixed layer that formed on the surface, perhaps due to wind stresses or surface stresses exerted by the disk. The density of the step was used to define a g' for the step (with the respect to the density at the surface). Figure 11 also shows how the thickness of the step, ΔZ, was defined. Figure 12 shows a typical density profile for the same B as in Figure 11, but now with upwelling. The depth predicted by Bush and Woods is still shown. It is apparent that the plume did not descend as deep as in the case without upwelling. The intrusion was also much thicker. Comparison with the lower photo in Figure 10 confirms that the plume mixed more as it descended when upwelling was present. Figure 13 combines the typical profiles of the background, the intrusion without upwelling (plume), the background with upwelling, and the intrusion with upwelling (upwelling). The important thing to note is the differences in the structure of the density step with and without upwelling. Another important fact is that the background density profile does not change dramatically once the upwelling begins.

Figure 14 shows the measured depth of the midpoint of the intrusion plotted in dimensionless form using the scaling of Bush and Woods (Equation 1). Note that for the points where there was no upwelling, M was taken to be 1, although in reality it is 0 and the value of B/M at these points is infinite. The points with the lowest values of B/M were discarded because the midpoint of the intrusion was less than the depth of the mixed layer at the surface after upwelling started but before the plume was injected. Hence it was not possible to discern between the mixed layer and the intrusion. The figure shows the depth of the mixed layer for each experiment. An attempt was made to determine a relationship between the depth of the midpoint and B/M. The relationship needed to asymptote to a constant value as B/M went to $+\infty$ in order to match the results of Bush and Woods and tend to zero as B/M got smaller. The data was fit to a form

$$\frac{Z_n N}{(B/L)^{1/3}} = C_1 exp\left(-C_2 M/B\right), \tag{18}$$

where C_1 and C_2 are constants that were determined to be 2.6 and 0.02, respectively. The value of 2.6 is the asymptote that the data approaches as B/M becomes infinite, which is the same condition as the experiments of Bush and Woods. The value of 2.6 is smaller than their average value of 3.0, but within their stated range. The current value is also very

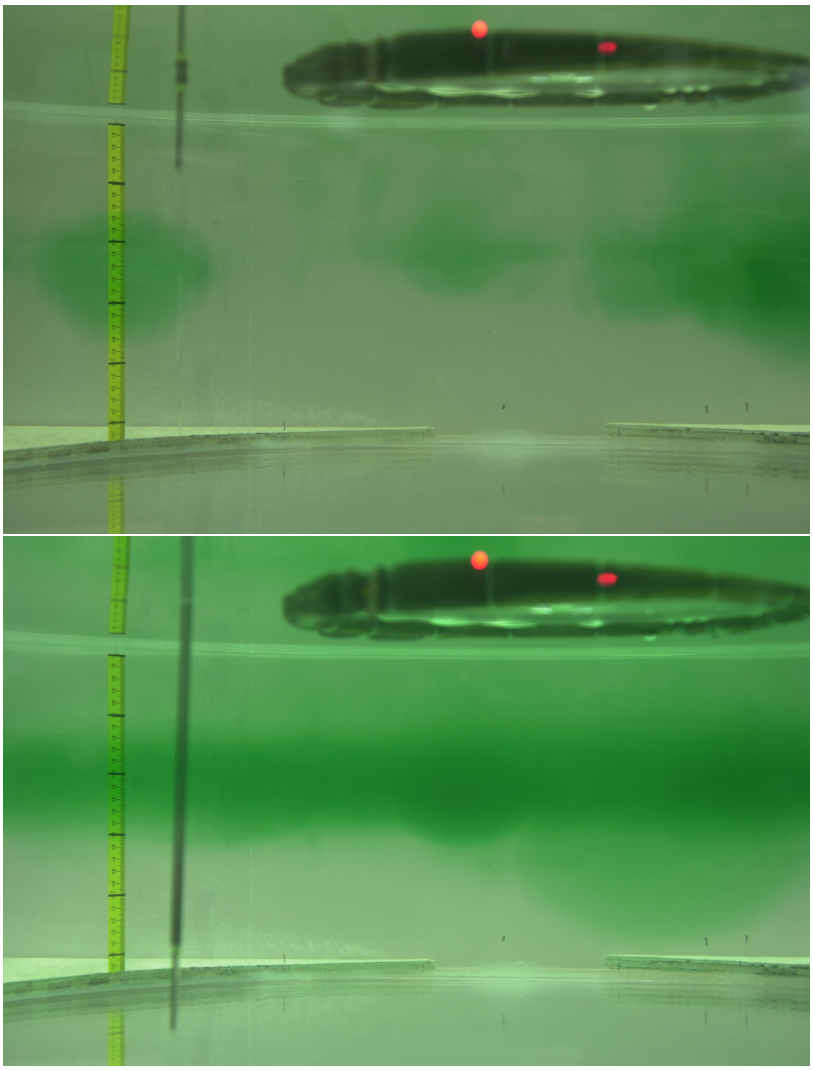

Figure 9: Behavior of a plume with no upwelling ($B = 400\ cm^4 s^{-3}$) after one injection (upper photo) and five injections (lower photo).

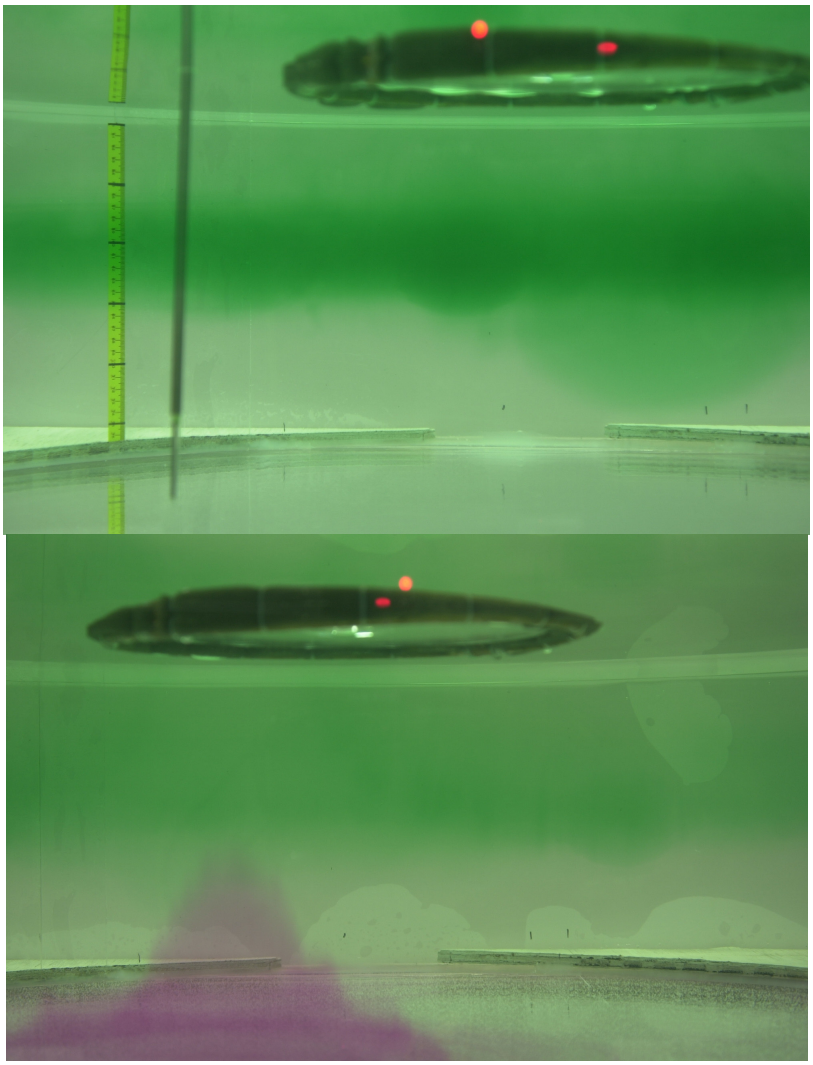

Figure 10: Comparison of plume behavior in the plume only case (upper photo) and the plume in the presence of upwelling (lower photo). All the parameters were the same between the two photos and they were both taken after five injections. $B/M = 0.02$ in the lower photo. The purple potassium permanganate on the bottom of the lower photo shows the upwelling.

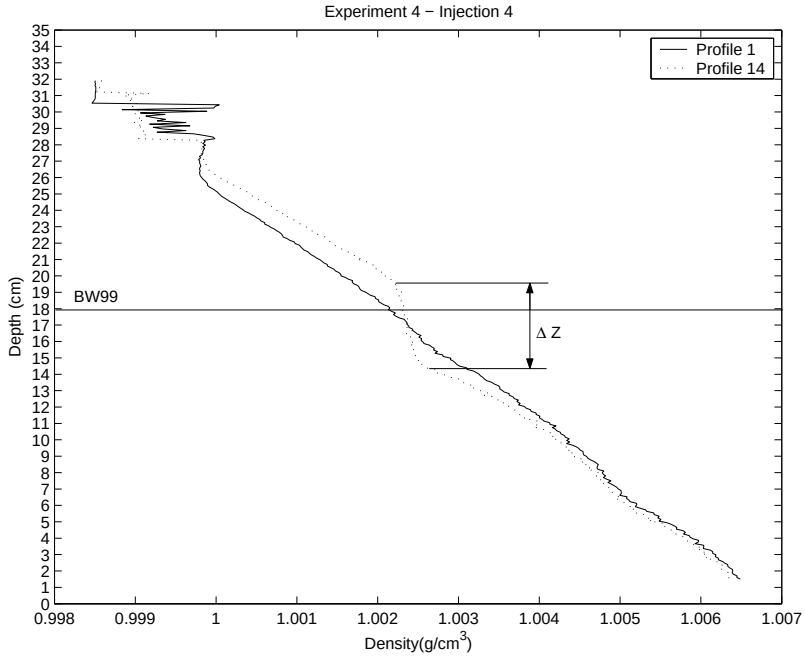

Figure 11: Density profile for a plume with no upwelling ($B = 220\ cm^4 s^{-3}$). The definition of the density step is shown as well as the depth of the intrusion as predicted by Bush and Woods. Profile 1 is the background density profile before injection. In this experiment the mixed layer is seen to extend to 26 cm.

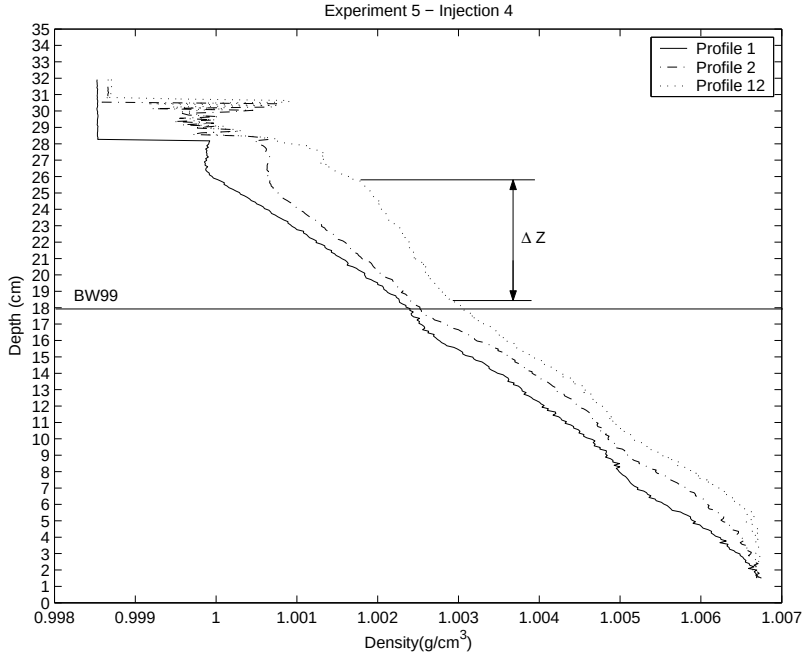

Figure 12: Density profile for a plume with upwelling ($B/M = 0.02$). Profile 1 is the background density profile before injection and prior to starting the disk. Profile 2 is the density profile after the disk was started but prior to injection.

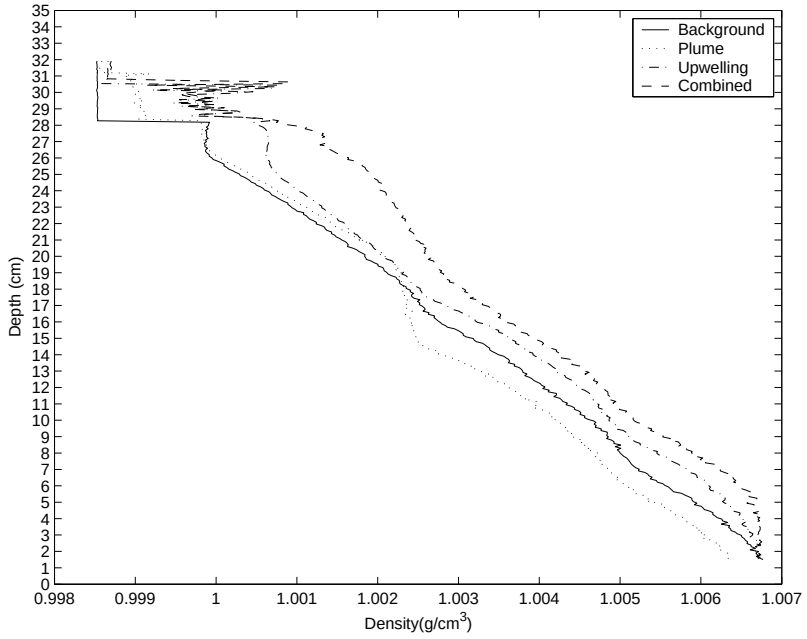

Figure 13: Summary of typical density profiles seen in the current experiments.

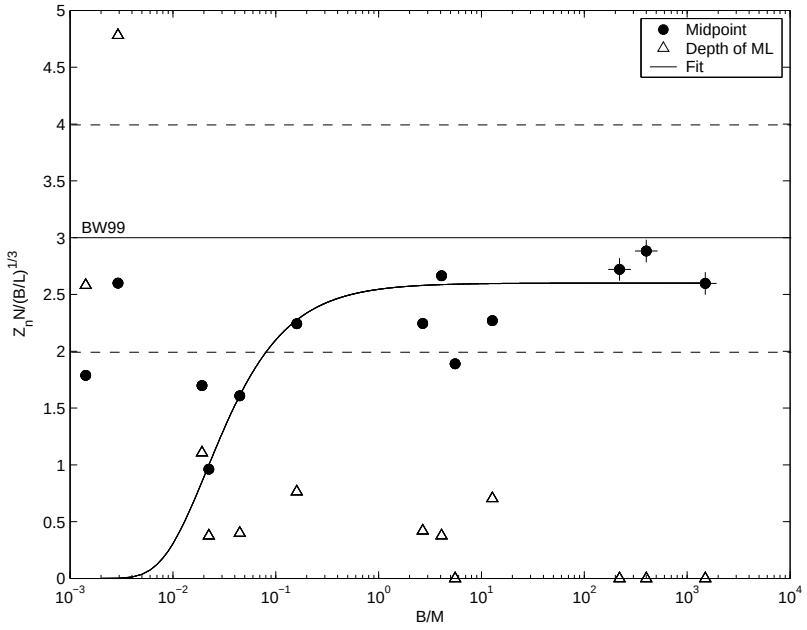

Figure 14: Depth of the intrusion due to the plume. The circles indicate the measured depth and the triangles indicate the depth of the mixed layer. The predicted value of the dimensionless depth from Bush and Woods is shown as a solid line with its margin of error showed as dashed lines. The data points with crosses indicate the points with no upwelling, and hence an infinite B/M.

similar to the value of 2.5 found by Wright and Wallace for the nonrotating case. In general the depth of the intrusion decreased with decreasing B/M, which is compatible with the hypothesis that as M increases the plume mixes more quickly and thus does not descend as deeply.

Figure 15 shows g_i' of the step normalized by the scaling of Bush and Woods (Equation 3). While there was much scatter in this data, there was a general increase in the dimensionless reduced gravity with B/M. This was the expected trend because as B/M decreased, the plume did not descend as deep, thus the density at its neutral level was closer to the density at the surface.

Figure 16 shows the thickness of the step normalized by the predicted height of the eddies created by the upwelling from Equation 7. Note that the experiments that had no upwelling are excluded from this figure because h_e is undefined in these experiments. For $B/M < 1$, the normalized thickness was essentially constant. This is consistent with the eddies from the upwelling having a great effect on the plume behavior in this regime. As B/M increased, the eddies had less of an effect on the structure of the intrusion. This is confirmed by examining the dimensionless thickness as a function of B and M individually. Figure 17a shows that there was no obvious dependence on B. Figure 17b shows that the trend observed in Figure 16 is due to changes in M. Hence, the thickness of the step was correlated with the strength of the lateral eddy buoyancy flux for $B/M < 1$.

Lastly, the proposed effective buoyancy flux from Equation 17 was evaluated. The

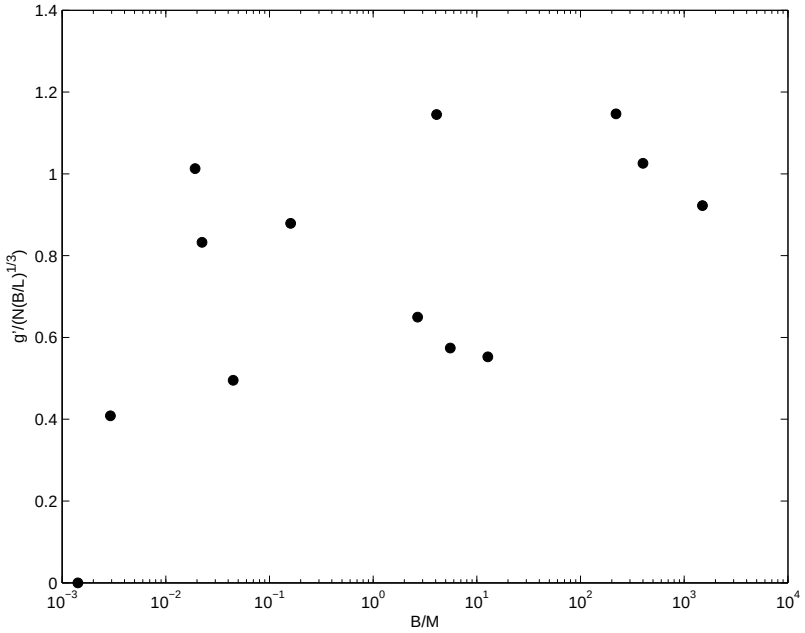

Figure 15: Reduced gravity of the intrusion with respect to the surface density.

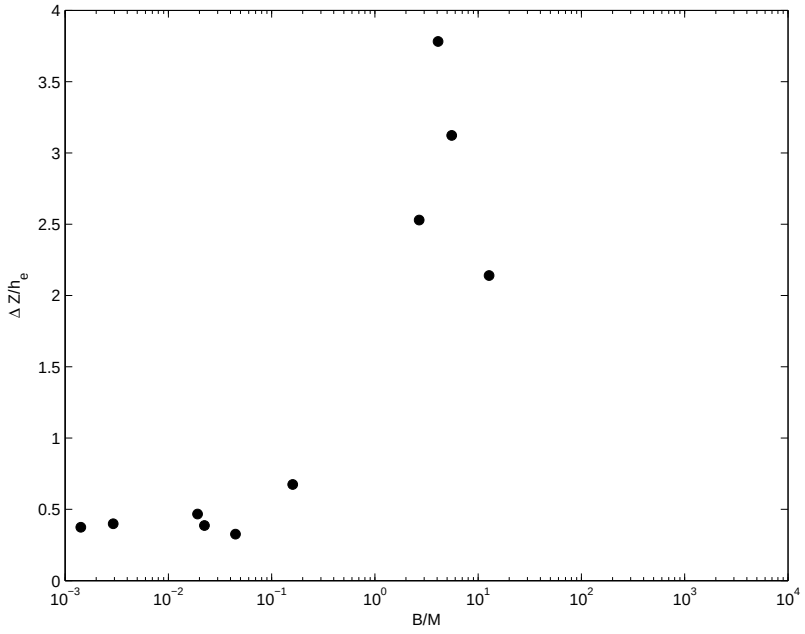

Figure 16: Thickness of the intrusion.

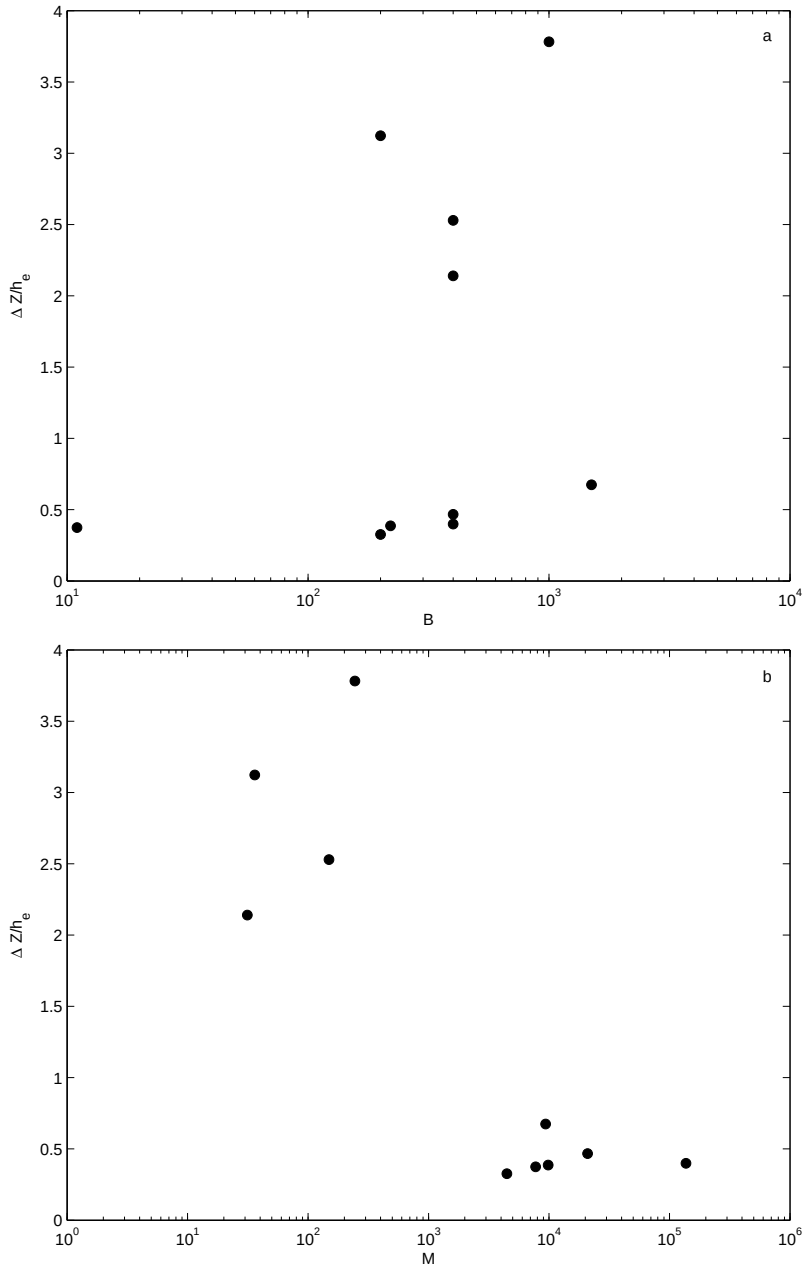

Figure 17: Thickness of the intrusion as a function of B and M independently.

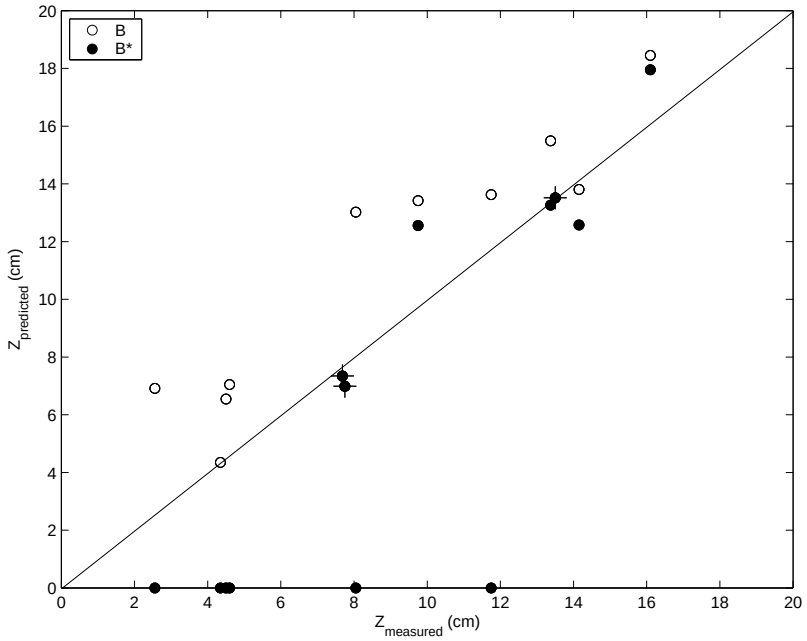

Figure 18: Comparison of the predictions of the intrusion depth using the standard buoyancy flux as defined in Equation 8 and the effective buoyancy flux defined in Equation 17. The dashed line indicates the line of equality between the measured and predicted values. The data points with crosses indicate the points with no upwelling and hence $B* = B$. Note that the points along the x-axis are due where the effective buoyancy flux is not valid.

theoretical intrusion depth was computed using the scaling of Bush and Woods with a coefficient of 2.6 instead of 3.0 to better fit the current data (see Equation 1). Figure 18 compares how the scaling performs with B as defined in Equation 8 and $B*$ as defined in Equation 17. Note that one limitation of this formulation is that it is not valid for $B/M < 1$, which limits its application when the lateral eddy buoyancy flux is expected to dominate. For the remaining points, in general there is an improvement when using the prediction with the effective buoyancy formulation.

5 Discussion

To gain insight into the formation of EDW, the ratio B/M in this region was computed. From the heat flux in Figure 1, the buoyancy flux per unit area was determined to be 10^{-7} $m^2 s^{-3}$. From this figure, the surface area (SA) over which this flux acts was measured to be 1000 km by 200 km. A typical velocity for the Gulf Stream is 1 ms^{-1} and a typical depth over which the gulf stream acts is 1 km. The Rossby radius of deformation in this region is on the order of 100 km. The value of N/f in this region ranges between 30 and 100, so typical stratifications are between $N = 3 \times 10{-}3$ and 10^{-2} s^{-1}. The cross sectional area (CSA) through which the lateral eddy buoyancy flux moves is the length of this zone times the depth of the gulf stream. So

$$B = B/area \times SA = 2 \times 10^4 m^4 s^{-3}$$
$$M = cVN^2H \times CSA = 2 - 5 \times 10^6 m^4 s^{-3}$$

giving a value of $B/M = 4 \times 10^{-3}$ to 10^{-2}. Based on the current experiments, the EDW zone falls into the regime where eddies from the Gulf Stream dominate and the properties of the plume were not important. The effective buoyancy flux formulated above could not be used here because of the low value of B/M. While the EDW falls into this regime, interestingly even the Bush and Woods scaling, which does not account for the lateral eddy fluxes, underestimated the depth of the the EDW, predicting a depth of $80 - 270\ m$ (depending on N/f). The EDW is typically seen between 200 and 500 m, so towards the lower end of the ratio of N/f, predictions approach the observations. Note that in the current experiments, N/f ranged between 0.1 and 1. Another possible explanation for the shallower intrusion depth predicted could be due to the use of a seasonally averaged buoyancy flux on the surface. Using a time averaged buoyancy flux through an entire experiment reduced the B/M values from the lab by a factor of 100, putting the estimated values from the ocean in the middle of the range investigated in the experiments. It is not clear if this is more physically appropriate, as the instantaneous plume properties may be what controls the intrusion behavior, not the time averaged plume properties.

6 Conclusion

Laboratory experiments were conducted to investigate behavior of a dense plume in a rotating linearly stratified fluid in the presence of eddies created by a baroclinic unstable front. The purpose of the experiments was to simulate the formation of Eighteen Degree Water to gain insight into the properties of this mode water. The vertical and lateral eddy buoyancy fluxes were estimated and their ratio, B/M, used to determine properties of the intrusion formed from the plume. The depth of the intrusion was found to be smaller in the presence of eddies from the baroclinic front. An effective buoyancy flux was defined that improved predictions of the depth of the intrusion as long as $B/M > 1$. Further analysis of the scaling for B and M is necessary before application to Eighteen Degree Water can be successfully made.

7 Acknowledgements

I would like to thank the GFD program for giving me the opportunity to be here this summer, Claudia Cenedese for the idea behind the experiments and all her time and guidance, John Marshall for help with the scaling and the theory, and Keith Bradley for setting up the rotating table, fixing all the things that kept breaking while I was running these experiments, and conversation during those long hours in the lab. I would also like to thank the 2-m rotating table for only trying to kill me once. Lastly I want to give mad props to my officemates and the other fellows for constant entertainment and helping me get through the requisite all-nighters to complete this project, when Diet Dr. Pepper alone would not suffice. Marshall gets a special shout out for being my lab buddy and for being such a help with my figures.

References

[1] K. Speer and E. Tziperman, "Rates of water mass formation in the North Atlantic ocean," J. Phys. Ocean. **22**, 93 (1992).

[2] Y.-O. Kwon and S. C. Riser, "Observations of the north atlantic subtropical mode water," First ARGO Science Workshop (2003).

[3] T. Joyce, A. Hernandez-Guerra, and W. Smethie, "Zonal circulation in the NW Atlantic and Caribbean from a meridional World Ocean Circulation Experiment hydrographic section at 66 degrees W," J. Geophys. Res. **106**, 22095 (2001).

[4] H. Rouse, C. Yih, and H. Humphreys, "Gravitational convection from a boundary source," Tellus **4**, 201 (1952).

[5] B. Morton, G. Taylor, and J. Turner, "Turbulent gravitational convection from maintained and instantaneous sources," Proc. Roy. Soc. London **234**, 1 (1956).

[6] S. Wright and R. Wallace, "Two-dimensional buoyant jets in stratified fluid," J. Hydraul. Div. Am. Soc. Civ. Eng **105**, 1393 (1979).

[7] Y. Noh, H. Fernando, and C. Ching, "Flows induced by the impingement of a 2-dimensional thermal on a density interface," J. Phys. Ocean. **22**, 1207 (1992).

[8] C. Ching, H. Fernando, and Y. Noh, "Interaction of a negatively buoyant line plume with a density interface," Dyn. Atmos. Oceans **19**, 367 (1993).

[9] H. Fernando and C. Ching, "Effect of background rotation on turbulent line plumes," J. Phys. Ocean. **23**, 2125 (1993).

[10] J. Lavelle and D. Smith, "Effects of rotation of convective plumes from line segments sources," J. Phys. Ocean. **26**, 863 (1996).

[11] H. Fernando, R. r. Chen, and B. Ayotte, "Development of a point plume in the presence of background rotation," Phys. Fluids **10**, 2369 (1998).

[12] J. Bush and A. Woods, "Vortex generation by line plumes in a rotating stratified fluid," J. Fluid Mech. **388**, 289 (1999).

[13] K. Helfrich and T. Battisti, "Experiments on baroclinic vortex shedding from hydrothermal plumes," J. Geophys. Res. **96**, 12511 (1991).

[14] K. Speer and J. Marshall, "The growth of convective plumes at sea-floor hot-springs," J. Geophys. Res. **96**, 12511 (1991).

[15] S. Narimousa and T. Maxworthy, "2-layer model of shear-driven coastal upwelling in the presence of bottom topography," J. Fluid Mech. **159**, 503 (1985).

[16] S. Narimousa and T. Maxworthy, "Coastal upwelling on a sloping bottom - the formation of plumes, jets, and pinched-off cyclones," J. Fluid Mech. **176**, 169 (1987).

[17] C. Cenedese, J. Marshall, and J. Whitehead, "A laboratory model of thermocline depth and exchange fluxes across circumploar fronts," J. Phys. Ocean. **34**, 656 (2004).